



# Chemistry A European Journal

 **Chemistry  
Europe**  
European Chemical  
Societies Publishing

## Accepted Article

**Title:** Effect of Stereochemistry on the Supramolecular Self-Assembly  
Chirality and Gelation Property

**Authors:** Minggao Qin, Yaqian Zhang, Chao Xing, Li Yang, Changli  
Zhao, Xiaoqiu Dou, and Chuan Liang Feng

This manuscript has been accepted after peer review and appears as an Accepted Article online prior to editing, proofing, and formal publication of the final Version of Record (VoR). This work is currently citable by using the Digital Object Identifier (DOI) given below. The VoR will be published online in Early View as soon as possible and may be different to this Accepted Article as a result of editing. Readers should obtain the VoR from the journal website shown below when it is published to ensure accuracy of information. The authors are responsible for the content of this Accepted Article.

**To be cited as:** *Chem. Eur. J.* 10.1002/chem.202004533

**Link to VoR:** <https://doi.org/10.1002/chem.202004533>

WILEY-VCH

# Effect of Stereochemistry on the Supramolecular Self-Assembly Chirality and Gelation Property

Minggao Qin<sup>1</sup>, Yaqian Zhang<sup>1</sup>, Chao Xing<sup>1</sup>, Li Yang<sup>1</sup>, Changli Zhao<sup>1</sup>, Xiaoqiu Dou<sup>1</sup>,  
Chuanliang Feng<sup>1,\*</sup>

State Key Lab of Metal Matrix Composites, School of Materials Science and Engineering, Shanghai Jiao Tong University, 800 Dongchuan Road, Shanghai 200240, China

\*Corresponding author

Tel: +86-021-54747651; E-mail: clfeng@sjtu.edu.cn

## Abstract

Although chiral nanostructures have been fabricated at various structural levels, the transfer and amplification of chirality from molecules to supramolecular self-assemblies are still puzzling, especially for heterochiral molecules. Herein, four series of C<sub>2</sub>-symmetrical dipeptide-based derivatives bearing various amino acid sequences and different chiralities are designed and synthesized. The transcription and amplification of molecular chirality to supramolecular assemblies are achieved. The results show that the supramolecular chirality is only determined by the amino acid adjacent to the benzene core and irrespective of the absolute configuration of C-terminal amino acid. In addition, the molecular chirality also has a significant influence on their gelation behaviors. For the diphenylalanine-based gelators, the homochiral gelators can be gelled through conventional heating-cooling process, while heterochiral gelators form translucent stable gels under sonication. And the racemic gels possess higher mechanical properties than that of pure enantiomers. All these results contribute to an increasing knowledge over control the generation of specific chiral supramolecular structures and the development of new optimized strategies to achieve functional supramolecular organogel through heterochiral and racemic systems.

## Introduction

Chirality is a ubiquitous phenomenon in nature from the microscopic to the macroscopic scale.<sup>[1-4]</sup> Usually, chiral molecular units can decide both molecular conformations and supramolecular biological functions.<sup>[5, 6]</sup> Inspired by the specific chirality in life processes, the design and fabrication of chiral nanostructures as well as their applications in the fields of asymmetric catalysis<sup>[7, 8]</sup>, enantiomer discrimination or sensor<sup>[9, 10]</sup>, biological effects<sup>[11, 12]</sup>, and optical materials<sup>[13]</sup> have been tremendously reported. However, the establishment of clear rules for achieving an accurate knowledge on the chiral amplification in self-assembling systems is still challengeable.<sup>[14-17]</sup> Revealing the fundamental discipline about the chiral amplification from simple molecules towards supramolecular assembled nanostructures would be of significance in guiding us in construction chiral supramolecular materials.<sup>[18]</sup>

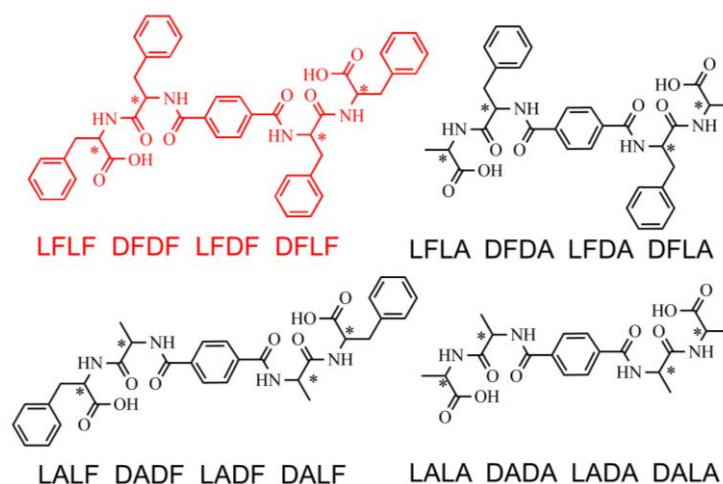
To date, various chiral nanostructures such as helical ribbons,<sup>[19-21]</sup> twisted nanofibers,<sup>[22-25]</sup> rolled-up nanotubes,<sup>[26-28]</sup> and even super-helix<sup>[29-31]</sup> have been constructed. For two-component co-assembly systems, the chiral amplification is usually obedient to the following rules: (i) sergeants-and-soldiers (S&S) effect,<sup>[32]</sup> (ii) majority-rules (MR) effect,<sup>[33]</sup> and (iii) diluted MR effect,<sup>[34]</sup> a combination of the above two effects. In comparison, the situation is more sophisticated for self-assembly of single component. In most cases, left-handed chiral nanostructures drive from peptides composed of L-amino acids, whereas D-amino acid derivatives are prone to self-assemble into right-handed twist or helix.<sup>[31, 35]</sup> However, it is still difficult to predict the self-assembled supramolecular chirality based on a known peptide sequence which contains more than one chiral center.<sup>[15-17]</sup> Recently, some intriguing investigations on chiral amplification phenomenon are reported.<sup>[36-38]</sup> For example, Xu and co-workers investigated the self-assembly chirality of three pairs of short tetrapeptide enantiomers, and found that the handedness of the supramolecular nanofibrils was determined by the chirality of the hydrophilic Lys head at the C-terminal, while the morphological handedness could not be changed by altering the molecular chirality of hydrophobic Ile residues.<sup>[16]</sup>

Apart from the effect of molecular chirality on its self-assembled handedness, chirality is proved to be not a pre-requisite but an effective parameter to regulate gelation properties.<sup>[39-41]</sup> It has been widely accepted that homochiral peptide-based gelators are more prone to gelate compared with heterochiral molecules, results in thermally and mechanically robust homochiral self-assemblies.<sup>[42]</sup> The investigation of D-amino acids, especially the combination of L- and D-amino acids is largely overlooked. It is only in last few years that heterochiral molecules have attracted more and more attention due to their unusual self-assembling behaviors and great potential biological applications.<sup>[43-45]</sup>

Herein, based on C<sub>2</sub> symmetrical molecular system, a rule of chiral transfer and amplification from molecules to supramolecular assemblies is established, as well as the effect of stereochemistry on gelation property is investigated. 16 molecules in which two dipeptide arms with different sequences and chiralities connected to para-disubstituted phenyl group are design and synthesized (Scheme 1). For this system, the supramolecular chirality is just determined by the chirality of amino acid close to the benzene core, not related to the terminal one. In addition, for the diphenylalanine-based gelators, the homochiral gelators can be gelled through conventional heating-cooling process and heterochiral gelators form translucent stable gels under sonication, which has been rarely reported. This work not only deepens our fundamental understanding on the transfer and amplification of molecular chirality to supramolecular chirality, but also provides an easy accessible approach to fabricate chiral organogels for potential applications.

## Results and discussion

In this study, 16 molecules are designed and synthesized according to the reported literatures (Scheme 1)<sup>[10]</sup>. All the synthesized compounds were characterized by <sup>1</sup>H and <sup>13</sup>C NMR spectra, high-resolution mass (Figure S4-S19), as well as their melting points (Table S1) and FT-IR spectra (Figure S22).



**Scheme 1.** Molecular structures of 16 molecules in which two dipeptide arms with different amino acid sequences and chiralities conjugated to para-disubstituted phenyl group; F: phenylalanine, A: alanine, L and D represent L- and D-amino acids.

### Molecular chirality effect on self-assembled handedness

All the gelators were initially dissolved in ethanol through heating, allowing them to self-assemble when cooling down under room temperature. SEM images showed micrometer-long twisted fibers assembled from the as-prepared dipeptide-based derivatives (Figure 1). Left-handed nanofibers (M) separately assembly from LFLF, LFLA, LALF, and LALA, while right-handed nanofibers (P) were obtained from DFDF, DFDA, DADF, and DADA. Obviously, the molecular chirality played a decisive role in determining the supramolecular chirality. The results were accordance with the previous reports that L-type amino acid derivatives are preferred to generate left-handed twist or helix, and vice-versa.<sup>[31]</sup> More intriguing, all the heterochiral gelators with L-amino acid adjacent to phenyl core and D-amino acid at terminal (LFDF, LFDA, LADF, and LADA) possessed left-handed nanofibers. On the contrary, the remaining four heterochiral enantiomeric molecules (DFLF, DFLA, DALF, and DALA) revealed right-handedness.

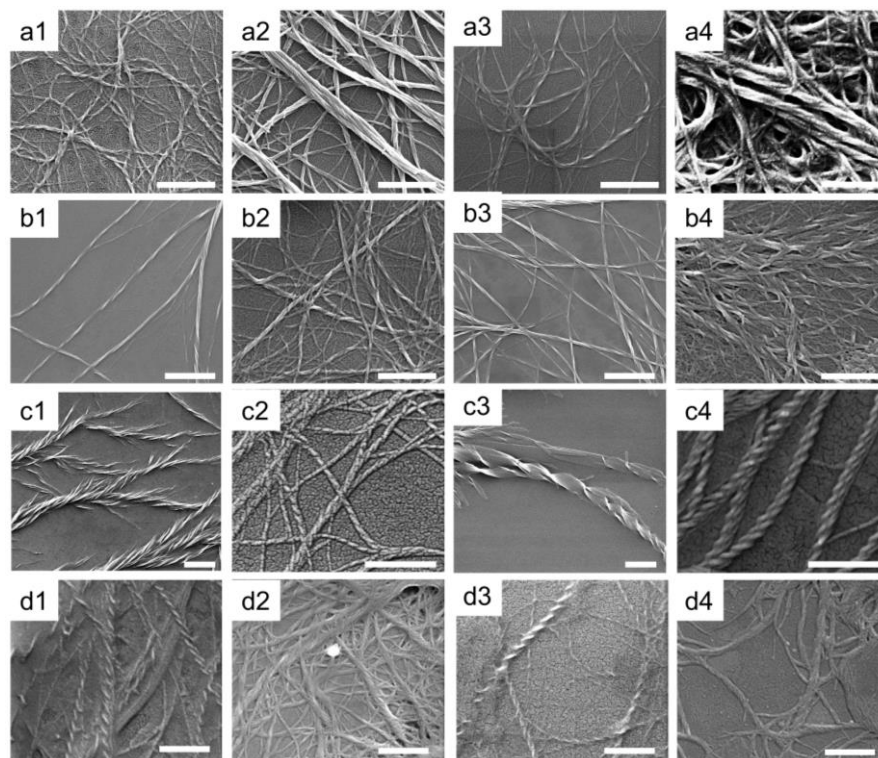


**Figure 1.** SEM images of supramolecular self-assemblies. Left-handed (M) nanofibers assembled from (a1) LFLF, (a2) LFDF, (b1) LFLA, (b2) LFDA, (c1) LALF, (c2) LADF, (d1) LALA, and (d2) LADA, and right-handed (P) nanofibers assembled from (a3) DFDF, (a4) DFLF, (b3) DFDA, (b4) DFLA, (c3) DADF, (c4) DALF, (d3) DADA, and (d4) DALA were presented. Scale bars: 500 nm for c2, c4 and d1-d4, 1  $\mu\text{m}$  for the other cases.

With changing the chirality of the amino acid near to the benzene core, nanofibers with reversed handedness were formed. On the contrary, the helicity would not change with altering the chirality of the C-terminal amino acids. The above SEM results clearly indicated that the supramolecular chirality was solely determined by the chirality of the amino acid adjacent to the benzene core, irrespective of the absolute configuration of the terminal amino acid. This finding was contradictory to some preceding reports that the supramolecular chirality was dictated by the C-terminal chirality which was called “C-terminal rule”.<sup>[46-48]</sup> In fact, the gelators in those systems were amphiphilic molecules and upon self-assembly the C-terminal hydrophilic head group residues were located on the surface of the self-assembled aggregates. It could be anticipated that terminal noncovalent interactions among gelators or solvents play a profound effect on controlling the supramolecular morphology, as well as handedness.<sup>[16]</sup> Here, the

prepared non-amphiphilic and the use of organic solvent were not suitable to this “C-terminal rule”.

Even though the changes of amino acids sequence were not found to prevent the impartation of chirality onto the nanofiber handedness, subtle differences were observed. For Phe-Phe enantiomers, homochiral LFLF and DFDF respectively showed uniform left and right-handed nanofibers with similar diameter and helical pitch. However, the helix was not distinct for heterochiral LFDF and DFLF and only a few nanofibers showed helix structure, demonstrating the vital effect of amino acid chirality. The homologous phenomenon was also occurred for Phe-Ala enantiomers. Interestingly, the helix were noticeable for all four Ala-Phe enantiomers. Homochiral LALF and DADF showed single twisted, while heterochiral LADF and DALF presented superhelix composed of single helix. Compared with the other three systems, the nanofibers exhibited smaller sizes for Ala-Ala enantiomers due to their smaller amino acid residues.

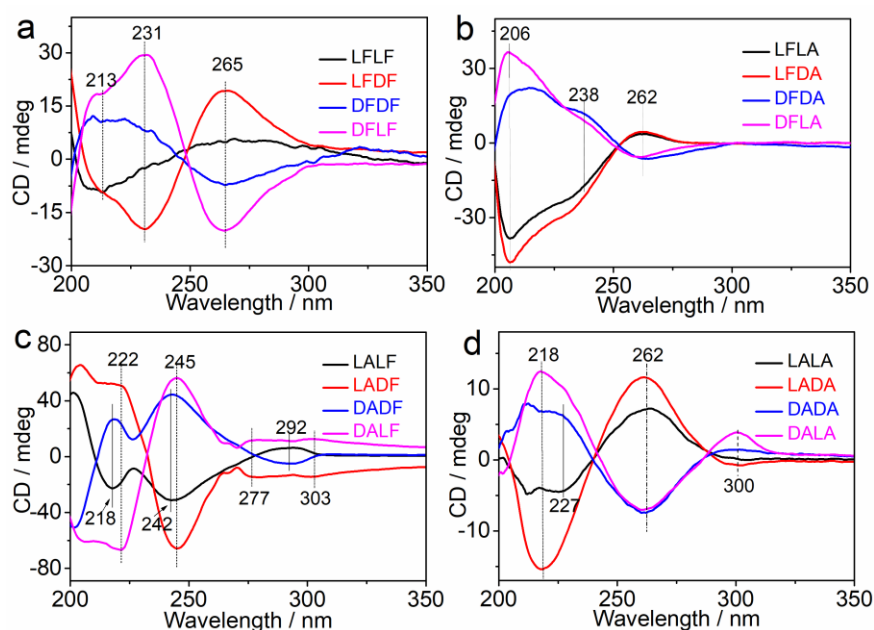


**Figure 2.** CD spectra of self-assembled membranes obtained from solutions evaporation on quartz plates under room temperature: (a) LFLF, LFDF DFDF, DFLF; (b) LFLA, LFDA, DFDA, DFLA; (c) LALF, LADF, DADF, DALF; (d) LALA, LADA, DADA, DALA.

It is well-known that circular dichroism (CD) spectra appear when the chromophoric moieties of chiral molecules are organized into an appropriate orientation.

The inherent chirality present in the dipeptide-based gelators and the specific stacking modes of the amide carbonyl and benzene groups allowed the aggregated state to be studied by CD.

Initially, molecular chirality was characterized using a 1.0 mm quartz cuvette with concentration of 0.1 mg/mL, and their corresponding UV-Vis spectra were shown in Figure S20. The expected mirror-imaged CD spectra were acquired from the enantiomers in those four systems. Meanwhile, all the UV-Vis spectra possessed an absorption at around 248 nm due to the benzene chromophores. Upon self-assembly, an apparent red-shift of UV-Vis absorption and a new weak peak at around 290 nm were occurred (Figure S21), indicating the existence of intense intermolecular  $\pi$ - $\pi$  interactions.<sup>[49]</sup>

For Phe-Phe system (Figure 2a), the CD spectrum of LFDF displayed bisignate Cotton effect with a positive dichroic signal at 265 nm followed by a negative CD peak at 231 nm (sign: +/-). In contrast, DFLF showed perfect mirror images to LFDF with a negative signal at 265 nm and a positive signal at 231 nm (sign: -/+), indicating that the helical sense of the LFDF assemblies switched to opposite for DFLF. Similarly, the CD spectrum of LFLF possessed a positive Cotton effect at around 265 nm and a negative signal at around 213 nm (sign: +/-), which was opposite to the case of DFDF (negative minimum at 265 nm and positive maximum at about 215 nm (sign: -/+)). Notably, the occurrence of zero crossing located at around 245 nm corresponding to the maximum UV absorption, indicating that the strong exciton coupled aromatic chromophores were in a helical arrangement.<sup>[50, 51]</sup> That was, stronger interactions were existed within heterochiral chromophores than that of homochiral ones. On the other hand, compared with the CD spectra of self-assemblies, no exciton coupling occurred around 248 nm in solution state for all the four enantiomers (Figure S20a), indicating that tight  $\pi$ - $\pi$  stacking between the chromophores in self-assemblies might give rise to the formation of chiral helical nanofibers.

For the Phe-Ala (Figure 2b), the homochiral derivatives (LFLA and DPDA) and heterochiral derivatives (LFDA and DFLA) also showed mirror-image relationships to each other, respectively. Both LFLA and LFDA presented positive bisignate Cotton

effect with a positive dichroic signal at around 260 nm followed by a negative CD peak at 218 nm (sign: +/-) while DFDA and DFLA exhibited a negative dichroic signal at 262 nm and a positive one at 218 nm (sign: -/+), revealing distinctly opposite helicity. Similarly to Phe-Phe, all enantiomers of Phe-Ala showed split CD signals with a crossover at 252 nm. However, different to Phe-Phe derivatives which had almost equally strong splitting Cotton effects, the CD spectra of Phe-Ala derivatives possessed much weaker intensity around 262 nm than that of at 206 nm. It could be attribute to different orientation of the chromophores transition dipole moments existing in the Phe-Ala. Thus, for Phe-Phe, the exciton coupling most likely came from two identical chromophores of the benzene residues of the diphenylalanine, while for Phe-Ala, it might be due to the interaction between the benzene core and the benzene of phenylalanine adjacent to the core.

For Ala-Phe derivatives (Figure 2c), distinct differences of the CD spectra were occurred between homochiral (LALF, DADF) and heterochiral (LADF, DALF) enantiomers, suggesting the formation of two different molecular stacking models. The CD spectrum of the LALF displayed negative, negative, and positive Cotton signals at 218, 242, and 292 nm, respectively. Nevertheless, these three CD bands of DADF became positive, positive, and negative, indicating the formation of self-assemblies with opposite handedness. The Cotton signs at around 244 nm were associated with intramolecular transitions from the amide linkage to the central aryl group.<sup>[52]</sup> Moreover, CD signals appeared at higher wavelengths at 277, 292 and 303 nm could be assigned to the chiral scattering of light as a result of the interaction of the light with the chiral nanostructures.<sup>[51]</sup>

For the Ala-Ala molecules, the molecular CD spectra were shown in Figure S20g. Clearly, homochiral enantiomers LALA and DADA showed two main bands at 227 and 252 nm with opposite Cotton effects, and similar Cotton signals at 224 and 256 nm appeared in CD spectra of heterochiral enantiomers LADA and DALA. In comparison with the molecular CD signals at 227 and 252 nm, the CD curves of LALA and DADA assemblies also displayed the characteristic CD absorption at 227 nm (Figure 2d). A red-shift from 252 to 262 nm of LALA/DADA was observed, which was resulted from

the *J*-aggregation among molecules induced by H-bond interactions among the carboxyl groups. In view of heterochiral enantiomers LADA and DALA, besides the red-shifted peak at 262 nm, a blue-shift appeared from 224 to 218 nm due to the *H*-aggregation among molecules. Signals with positive or negative Cotton effects at 300 nm indicated the formation of helical superstructures with preferred handedness.<sup>[53]</sup> The peak at 262 nm was mainly due to intermolecular  $\pi$ - $\pi^*$  transitions of the central aryl group reported by previous study.<sup>[30]</sup>

As systematically demonstrated above, it revealed the chirality transformation from molecular scale into supramolecular level accompanied by the chirality amplification during the self-assembly process. More importantly, the handedness of the self-assembled nanostructures could be estimated and controlled based on a certain chirality of the molecule. The chiroptical activities of these self-assembled nanofibers were further determined by vibrational circular dichroism (VCD), which indicated the involvement of specific parts of the molecule configuration influenced by chiral supramolecular aggregation.<sup>[54]</sup> We conducted the VCD measurements by dropping the solution on a CaF<sub>2</sub> wafer followed by drying under ambient temperature overnight.

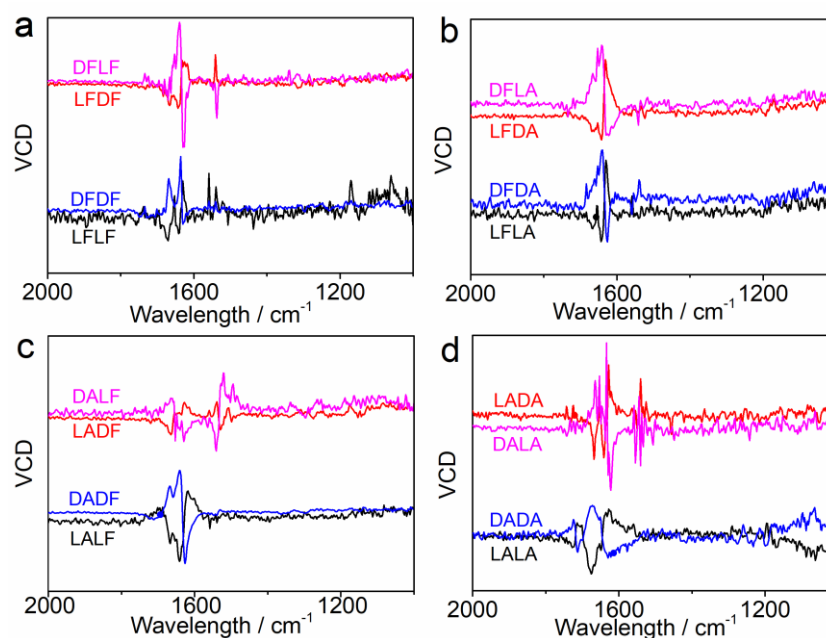


**Figure 3.** VCD spectra of membranes obtained from solutions evaporation on CaF<sub>2</sub> plates under room temperature: (a) LFLF, LFDF, DFDF, DFLF; (b) LFLA, LFDA, DFDA, DFLA; (c) LALF, LADF, DADF, DALF; (d) LALA, LADA, DADA, DALA.

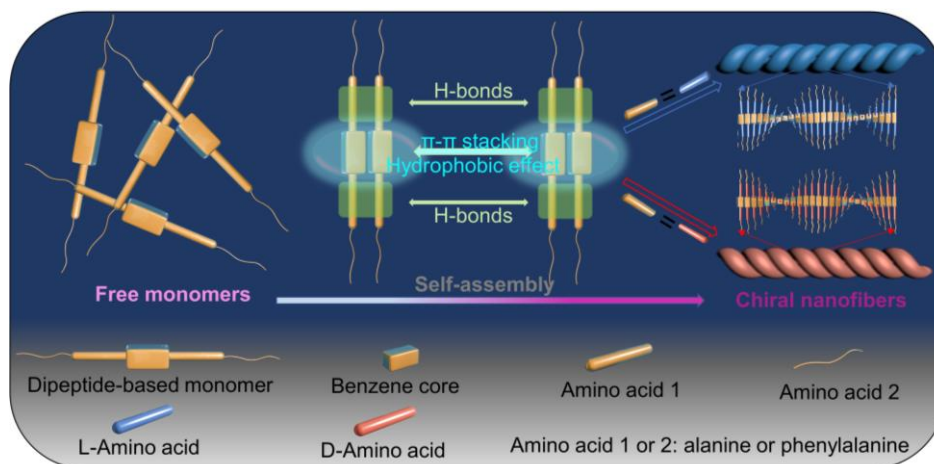
For Phe-Phe-based self-assembled systems (Figure 3a), LPLP and LPDP exhibited a (-/+) VCD signal of C=O stretching band between 1750 and 1600  $\text{cm}^{-1}$ , whereas the VCD signal of the band switched to a totally opposite (+/-) pattern for DPDP and DPLP assemblies. The VCD patterns indicated the opposite handedness of nanofibers assembled from LPLP/LPDP and DPDP/DPLP, which were in good accordance with the SEM and CD results. Moreover, a strong C=O $\cdots$ H-N hydrogen-bonding network was inferred from the vibrational amide I stretching band at around 1636  $\text{cm}^{-1}$ . The similar phenomena were occurred among Phe-Ala, Ala-Phe and Ala-Ala-based assemblies in Figure 3b, c and d, respectively. To be specific, the spectra of LPLP, LPDA, LALP, LADP, LALA, and LADA all showed -/+ signals in the range of 1750-1600  $\text{cm}^{-1}$  with left-handed self-assembled helices. Whereas right-handed nanofibers were formed from aggregation of DPDA, DPLA, DADP, DALP, DADA, and DALA, whose VCD spectra presented perfect mirror images (with a (-/+) pattern) to their corresponding enantiomers. These results suggested that the VCD signal patterns could be inversed by changing the chirality of the amino acid that adjacent to the molecular core, which further confirmed the crucial role of chirality of the specific amino acid in determining the helicity of the self-assemblies.

FTIR can provide critical information about the hydrogen bonds networks, especially in the region of 1800-1500  $\text{cm}^{-1}$ . The FTIR spectra of the products in their molecular states and assembled states were checked, as shown in Figure S22 and S23, respectively. Obviously, all the gelators show almost identical characteristic peaks at approximately 1723, 1676, 1652 and 1544  $\text{cm}^{-1}$ . The peak at 1723  $\text{cm}^{-1}$  is due to the C=O stretching vibration of carboxylic group. While, 1676 and 1652  $\text{cm}^{-1}$  of amide I and amide II at 1540  $\text{cm}^{-1}$  are attributed to the C=O stretching vibration and N-H bending vibration of the amide groups. And then, the KBr disk technique FTIR was used for the as-prepared self-assemblies, as shown in Figure S23a-d. Expectedly, almost the same spectra for homochiral and heterochiral molecules, respectively. Compared with the molecular states, the peaks of assemblies showed distinct shifts, indicating that the hydrogen bonding was one of the main driving forces for self-assembly. Besides, the multiple peaks emerged in amide I or II demonstrated the

existence of complex hydrogen bonds.

A feasible mechanism was proposed in Scheme 2. During self-assembly, the amide groups closed to the hydrophobic benzene core would be shielded from the solvent environment, thus allowing strong intermolecular H-bond formation to occur. Consequently, due to the directional hydrogen bonding and  $\pi$ - $\pi$  stacking, 1D molecular stacking further promoted the generation of nanofibers. Hence, the existence of specific stereochemistry of chiral chain residues suspended to the medial amide group would prefer to determine the handedness of the nanofibers. In comparison, the lateral amide groups were insusceptible to the phenyl core, but presumably to be affected by the adjacent hydrophilic carboxyl groups. This could explain the observation of various twisted nanofibers with different morphologies, diameters or helical pitches.

Overall, comprehensive characterizations (SEM, CD, VCD and FTIR) and interpretation of the nanostructures self-assembled from 16 C<sub>2</sub>-symmetrical molecules with various amino acid sequences and chiral centres were performed. It was showed that the chirality of amino acid proximal to benzene core determined the supramolecular chirality of the self-assembled nanofibers. This principle on chiral transformation and amplification was discrepant to the most previous literatures, in which the terminal chirality was dominant in controlling the handedness of assembled nanostructures. Even though the terminal amino acid chirality was insusceptible in regulating the supramolecular chirality, it impacted the nanofiber diameters, degree of twists, and helical pitches of the nanofibers. These results provided us a facile way to fabricate nanofibers with controllable chirality and tailored sizes by altering partial chirality and sequence of the involved amino acids.



**Scheme 2.** Schematic illustration showed the decisive role of chirality of amino acid close to benzene core (Amino acid 1) on the handedness of self-assembled nanofibers based on four series of dipeptide-based derivatives.

### Molecular chirality effect on gelation properties

Molecular chirality has been intensively proved to be a mysterious factor controlling its gelation behaviors. In most cases, homochiral molecules are more likely to be effective gelators than heterochiral ones, and racemates of the pure enantiomeric gelator mixtures are normally inclined to form precipitates rather than gels. In rare examples, all the enantiomers, diastereomers and racemates of a given dipeptide-based derivatives could form stable gels. Due to its structural simplicity, ease of chemical modification and biocompatibility, diphenylalanine (FF), a core recognition motifs of Alzheimer's  $\beta$ -amyloid polypeptide, has increasingly become subject of intense investigation in both sciences of medicine and nanotechnology. Herein, the synthesized LFLF, LFDF, DFDF, DFLF were utilized to investigate their gelation behaviours. Meanwhile, the racemates of homochiral enantiomers mixtures (MFMF) and heterochiral enantiomers mixtures (mFmF) were introduced. Noting that LFLF (DFDF) and LFDF/DFLF are diastereomers.

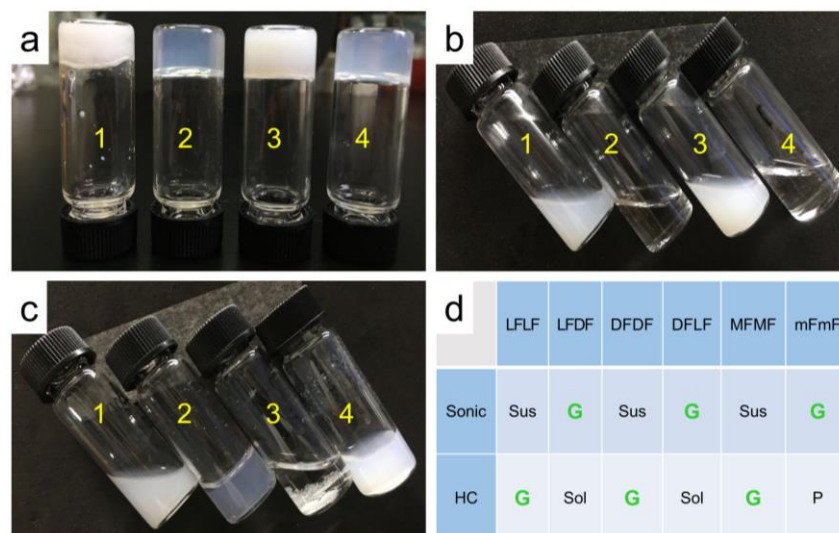


**Figure 4.** Photographs (a-c) showed gels formation results of LFLF, LFDF, DFDF, DFLF, MFMF and mFmF under heating-cooling or sonication methods. In (d), Sus: suspension, G: gel, Sol: solution, P: precipitate.

Homochiral enantiomers LFLF and DFDF formed into white opaque gels in ethanol through traditional heating-cooling (HC) method (Figure 4a1 and a3). Meanwhile, under the identical conditions, clear solutions were presented without any gelation tendency for LFDF and DFLF (Figure 4b2 and b4), and some sediments extracted from the solution were observed after 24 h (data not shown). It was not surprisingly that no gelation occurred to heterochiral enantiomers. However, homogeneous transparent organogels were obtained when LFDF or DFLF subjected to sonication for 2 min (Figure 4a2 and a4). We suggested that sonication initially accelerated the dissolution and dispersion of gelator molecules in ethanol, and then reorganized the molecules. It resulted in enhanced  $\pi$ - $\pi$  stacking between the aromatic groups and the intermolecular hydrogen bonding, providing the driving force to form extended supramolecular aggregates. In comparison, LFLF and DFDF exhibited white suspensions under sonication even with longer processing time (Figure 4b1 and b3). It demonstrated that the molecular chirality played a critical role in guiding their gelation abilities. These unusual phenomena had rarely been reported that the homochiral and heterochiral enantiomers gelled individually through heating-cooling and sonication. Inspired by this, we were intrigued to explore the gelation possibility of racemates under heating-cooling and sonication process. In Figure 4c1 and c4, MFMF displayed

suspension and white gel after dealing with sonication and heating-cooling, respectively. Semilucid organogel and precipitates were observed for mFmF (Figure 4c2 and c3). It was scarce that the racemates possessed similar gelation abilities with their related pure enantiomers.<sup>[55-59]</sup> Obviously, our observation expand the design rules to a more diverse toolbox of heterochiral peptides and even racemates, and opens the way to exciting possibilities for the fabrication of supramolecular architectures and functional materials.

To check how the different molecular chiralities were reflected in the macroscopic properties of these organogels, rheological tests were carried out to measure their mechanical rigidity. From a frequency sweep experiments with a constant strain 0.1% (Figure 5a), all the prepared organogels revealed stronger storage moduli ( $G'$ ) than relevant loss moduli ( $G''$ ), and also  $G'$  and  $G''$  values were weakly dependent on angular frequency over the range discussed. These data indicated the formation of stable organogels for all single gelators, as well as the enantiomeric mixtures. Furthermore, it was found that the mechanical strength as indicated by  $G'$  increased in sequence of LFLF $\approx$ DFDF $<$ MFmF $<$ LFDF $\approx$ DFLF $<$ mFmF (Figure 5b). From which three issues could be inferred. Firstly, enantiomeric pairs (LFLF/DFDF or LFDF/DFLF) had nearly equal storage moduli. Secondly, heterochiral enantiomeric pair possessed much higher storage moduli (around 2000 Pa) than homochiral enantiomeric pair (about 700 Pa). Thirdly, the organogels strength formed from racemates were obviously enhanced (about 1.5 times) compared with that of the gels formed by corresponding either pure enantiomers. These data also suggested that the enantiomers in the mixtures co-assembled into a new kind of network of mixed nanofibers, rather than self-sorting in the racemates gels.<sup>[60]</sup> Thus, we can conclude that altering molecular chirality and rearranging the D-amino acid in the appropriate position can be valuable approaches to regulate the mechanical strength of supramolecular gels.

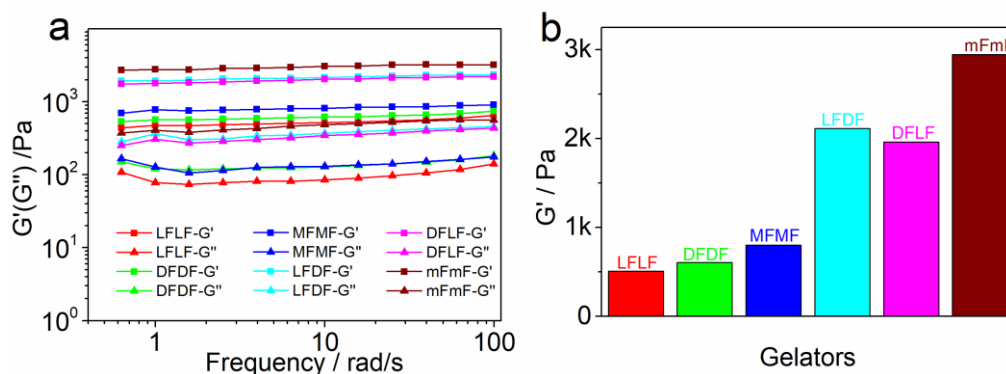


**Figure 5.** (a) Frequency sweeps of dynamic shear modulus for organogels made from LFLF, DFDF and MFMF after heating-cooling, and organogels made from LFDF, DFLF and mFmF under sonication, respectively. (b) Comparison of corresponding mechanical strength at a constant frequency of 6.29 rad/s.

The formation of gels was a synergetic effect of both gelator-gelator and gelator-solvent interactions, and the gel mechanical rigidity was dependent on both the number of crosslinks existed between fibrils in the network and the stiffness of the individual fibrils themselves. Subsequently, the self-assembled nanostructures were checked by scanning electron microscopy (SEM), which provides a visual way to estimate the impact of peptide stereoisomers on self-assembly.

Compared with the soluble winding nanofibers formed in ethanol (1 mg/mL) of homochiral enantiomers LFLF and DFDF (Figure 1a, c), stretching nanofibers in gel state were preserved (Figure 6a, c). Even though a slight change in morphology was emerged between solution and gel states, the supramolecular chirality remained the same, where LFLF and DFDF formed left- and right-handed twisted nanofibers, respectively. In contrast, distinct rigid nanofibers with much larger sizes were found in the gels of LFDF and DFLF (Figure 6b, d). Transmission electron microscopy (TEM) characterizations further confirmed the results displayed by SEM. Homochiral gelators reliably self-assembled into thin nanotwists with width of 30-50 nm and an average of helical pitches around 150-250 nm (insets of Figure 6a, b and S24a, c). Meanwhile, more rigid and thicker nanofibers with 100-150 nm in diameters and 400-500 nm in helical pitches were revealed (insets of Figure 6e, f and Figure S24b, d). As for the MFMF gels, nanofibers intertwined into wheel hub-like nanostructures, which possessed smaller

aspect ratio but larger sizes (Figure 6e). On account of mFmF gels, compact and entangled nanofibers were observed. Worth noting that the disappearance of twist both for MFmF and mFmF nanostructures further indicated the formation of co-assemblies. Besides, the self-assembled nanostructures of the non-gel systems were also conducted by SEM. No nanofibers but micro-scale worm-like aggregates were formed from homochiral enantiomers under sonication, as well as their racemates (Figure S25), which resulted in the occurrence of suspension rather than gels. The nanostructures of LFDF, DFLF produced nanofibers, and mFmF presented large bundles of fibers after heating-cooling (Figure S26).

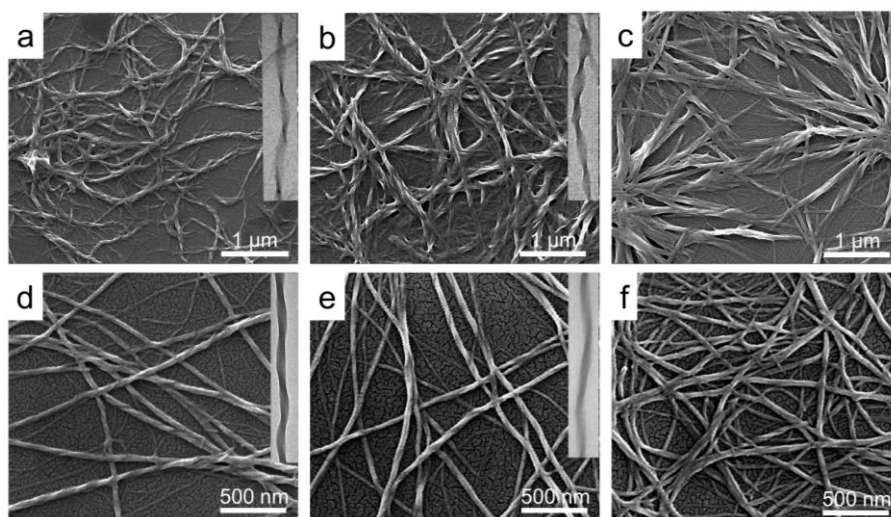


**Figure 6.** Morphologies of nanofibers based on organogels in ethanol: (a) LFLF, (b) DFDF, (c) MFmF, (d) LFDF, (e) DFLF, and (f) mFmF. Gels of a-c and d-f obtained by heating-cooling and sonication, respectively. Insets in a-b and d-e were their corresponding TEM images.

In view of the SEM results in concert with gelation behaviors and rheological strength, we could speculate that the molecular chirality significantly affect the intermolecular packing geometry, leading to distinct self-assembled nanostructures. Ultimately, these subtle alteration in morphologies could account for the differences observed in the corresponding macroscopic gelation behaviors. To better understand the gelation driving forces within the individual assembled gels, ATR-FTIR and temperature-dependent  $^1\text{H-NMR}$  were performed. On account of the identical gelation

abilities of enantiomeric pairs, the investigation on gelation mechanism were focused on LFLF, LFDF, MFMF and mFmF hereinafter.

FTIR spectra provide valuable information on the hydrogen bonding interactions. Herein, ATR-FTIR of the LFLF, LFDF, MFMF and mFmF organogels prepared with ethanol-D<sub>6</sub>, and their corresponding solution state in DMSO-D<sub>6</sub>, were detected carefully. All gelators in the monomer state presented nearly identical characteristic peaks at 1718, 1676, 1651 and 1543 cm<sup>-1</sup> (Figure 7a and S27). In comparison, distinct variations of spectra were obtained in their gel state. The peaks at around 1633 cm<sup>-1</sup> attributed to the hydrogen bonded stretching frequency of the amide group close to benzene core were presented in all gels, while the peak intensity for H-bonded amide C=O located in the periphery was much stronger for LFLF and MFMF gels than that within LFDF and mFmF gels. This indicated the existence of relative weaker hydrogen bonding interactions formed from terminal amide group among heterochiral gelators and their racemates. Meanwhile, the peaks in the range of 1750-1700 cm<sup>-1</sup> belong to C=O stretching vibration of terminal carboxyl groups displayed opposite shift tendency. A small bathochromic-shift occurred for LFLF and MFMF gels from 1718 to 1715 cm<sup>-1</sup>, while a significant hypochromatic shift happened to LFDF and mFmF gels from 1718 to 1730 cm<sup>-1</sup>. This result suggested that different intermolecular interactions originated from carboxyl were existed among the gelators, which likely to play a critical role on their gelation properties. Besides, compared with the single peak at 1541 cm<sup>-1</sup> assigned to amide N-H bending vibration in pure LFLF and LFDF gels, an obvious peak splitting phenomenon along with red-shift was emerged. This might be due to the stronger and multiple hydrogen bonds between enantiomers with opposite stereochemical centres in the racemic mixtures.

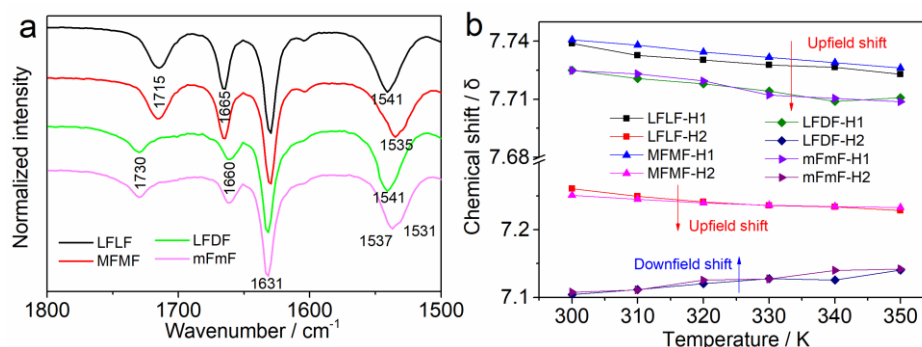


**Figure 7.** ATR-FTIR spectra and temperature-dependent  $^1\text{H-NMR}$  of LFLF, LFDF, MFMF and mFmF gels in ethanol-D<sub>6</sub>.

Apart from the different hydrogen bonds existed within the gels, it was rational to anticipate that aromatic interactions could be affected simultaneously owing to various chiralities. To verify this assumption, the temperature-dependent  $^1\text{H-NMR}$  experiments were further carried out on ethanol-D<sub>6</sub> gels. In the range of 7.8–7.0 ppm, two types of aromatic protons assigned to benzene core (H1: around 7.737 ppm) and phenylalanine residues (H2: around 7.260 ppm) were confirmed in the gel state at 300 K, respectively. When increasing temperature, along with the sharpening of the peaks, the both relevant peaks moved upfield gradually for all the four gels (Figure 7b and S28). Obviously, both these two benzenes were involved in aromatic interactions during the gelation of LFLF and MFMF. On the contrary, for LFDF and mFmF gels, H1 showed similar upfield shift with that of LFLF and MFMF, while H2 exhibited downfield shift unexpectedly. The different outcomes happened to phenylalanine residues were most likely to be the result of various  $\pi$ - $\pi$  stacking patterns, where LFLF and MFMF preferred to adopt *J*-aggregation, while *H*-aggregation were dominant in LFDF and mFmF gels.<sup>[61]</sup>

## Conclusions

In summary, four series of dipeptide-based derivatives with various amino acid sequences and chiral centres were designed and synthesized. The handedness of the twisted nanofibers was merely dictated by the chirality of amino acid conjugated to benzene core. The diameters and helical pitches could be facily regulated by altering the amino acid sequences and the stereochemistry of peripheral amino acid.

Furthermore, it was found that homochiral and heterochiral enantiomers could form organogels with the assistance of heating-cooling and sonication, respectively. However, suspension or solution (precipitates) instead of gels would be observed when reversing the processing methods. The decisive role of amino acid chirality on its supramolecular chirality and gelation properties could be attributed to the various hydrogen bonding, aromatic interactions and steric hindrance. The above observations on chiral transformation and amplification would be significantly beneficial in guiding us fabricate chiral nano-materials with desirable handedness and controllable sizes. In addition, the investigation of gelation property of dipeptide-based gelators, especially the heterochiral gelators and racemates would largely expand the potential applications due to the unique nature of D-amino acids.

## Experimental section

### Materials:

BOC-L/D-phenylalanine (BOC-L/D-Phe-OH), BOC-L/D-alanine, L/D-phenylalanine methyl ester hydrochloride (H-L/D-Phe-OMe HCl), L/D-alanine methyl ester hydrochloride, were purchased from J&K; 1-hydroxybenzotriazole (HOBt), N-(3-himethylaminopropyl)-n'-ethylcarbodiimide hydrochloride (EDCI), N,N-diisopropylethylamine (DIEA), 1,4-benzenedicarbonyl chloride, trifluoroacetic acid (TFA), dichloromethane (DCM), triethylamine (Et<sub>3</sub>N), methanol, sodium hydroxide (NaOH), sodium bicarbonate (NaHCO<sub>3</sub>), citric acid, sodium chloride (NaCl), those chemicals were purchased from Aladdin. All the chemicals used without further purification.

### Synthesis of Dipeptide-based Derivatives

The synthesis of the target products mainly involves four steps described in **Scheme S1** in Supporting Information. Take the preparation of LFLF as a typical example. Firstly, conventional solution-phase approaches for dipeptide synthesis were utilized: Boc-L-Phe-OH (2.66 g, 10 mmol), HOBt (1.76 g, 13 mmol), DIEA (5.56 g, 40 mmol) and H-Phe-OMe HCl (2.38g, 11 mmol) were dissolved in dry DCM (100 mL), and stirred under ice water bath for 30 min. EDCI (3.84 g, 20 mmol) was then added and the

mixture was further stirred for another 12 h. After washing successively with saturated citric acid solution, NaHCO<sub>3</sub> solution and brine, the obtained organic phase was dried over MgSO<sub>4</sub>. Purification through recrystallization (ethyl acetate/light petroleum) afforded BOC-L-Phe-L-Phe-OMe (3.62 g, 85%) (<sup>1</sup>H-NMR in Figure S1). Secondly, trifluoroacetic acid (TFA, 10.0 mL, 135 mmol) was added to a solution of BOC-L-Phe-L-Phe-OMe (3.62 g, 8.5 mmol) in dry DCM (10 mL). The reaction was quenched by adding an excess amount of methanol after 90 min. Evaporation of all solvents under vacuum afforded H-L-Phe-L-Phe-OMe (2.69 g, 97%) (<sup>1</sup>H-NMR in Figure S2). Thirdly, Et<sub>3</sub>N (5 mL, 36.45 mmol) was added to solution of H-L-Phe-L-Phe-OMe (2.69 g, 8.2 mmol) dissolved in dry CH<sub>2</sub>Cl<sub>2</sub> (50 mL), following by adding 1,4-benzenedicarbonyl dichloride (0.81 g, 4.0 mmol) dropwise. Precipitates formed overnight at room temperature, which was filtered off and washed in ethanol and dried to give pure product P-L-Phe-L-Phe-OMe (2.28 g, 71%) (<sup>1</sup>H-NMR in Figure S3). Finally, for the hydrolysis, aqueous NaOH (30 mL, 2M) was added to a cooled suspension of P-L-Phe-L-Phe-OMe (2.28 g, 2.9 mmol) in methanol (30 mL). The mixture was stirred for 24 hours at room temperature and acidified with 2 M HCl solution until pH value no more than 3.0. The precipitate was collected and dried under vacuum to give the product LFLF (1.82 g, 83%).

The other 15 molecules (LFDF, DFDF, DFLF, LFLA, LFDA, DFDA, DFLA, LALF, LADF, DADF, DALF, LALA, LADA, DADA, and DALA) with various amino acid sequences and chiral centres were synthesized in the same way for the synthesis of LFLF.

### Hydrogel Preparation.

LFLF (4.0 mg mL<sup>-1</sup>) was suspended in ethanol with a septum-capped 5.0 mL glass vial and heated until a transparent solution was obtained. The solution was turned into organogel after cooling to room temperature. The gels from DFDF and MFMF gelators could be obtained in the same way with LFLF gel. As for LFDF, DFLF and mFmF (4.0 mg mL<sup>-1</sup>), sonication were exerted for gel formation.

### Characterization of self-assemblies

#### Field emission scanning electron microscopy (FE-SEM)

FE-SEM measurements were carried out using an FEI QUANTA 250 microscope.

Samples were prepared by depositing the as-prepared solution (0.1 wt%) or gels (0.4 wt%) on silicon slice, dried in air at room temperature overnight and sprayed with a thin gold layer.

### **Transmittance electron microscopy (TEM)**

A 4  $\mu\text{L}$  aliquot of the sample was pipetted onto each grid. After 60 s adsorption the excess was wiped away using filter paper. Grids were dried under infrared lamp for 5 min. Samples were examined using a Tecnai G2 Spirit Biotwin at an operating voltage of 120 kV.

### **Circular dichroism (CD) spectroscopy**

The CD spectra of self-assemblies were measured using a JASCO J-815 CD spectrometer with bandwidth of 1.0 nm in the UV region (200-400 nm). For the CD of the film, in order to keep the film thickness same, we chose the quartz slide with a groove on it, and then fixed amount solution (100  $\mu\text{L}$ ) was added into the groove, and dried at room temperature. The molecular solution and organogel were measured in 0.1 mm quartz cuvette. Measurements were repeated 3 times to reduce the noise near 200 nm, their average were plotted.

### **Vibrational circular dichroism (VCD) spectra**

VCD spectra were obtained by BioTools using a ChiralIR-2X Fourier transform VCD (FT-VCD) spectrometer equipped with an MCT detector and the Dual PEM option for enhanced VCD baseline stability. VCD spectra were acquired at a resolution of 4  $\text{cm}^{-1}$  by co-adding 300 scans. The solution samples (at a concentration of 1.0  $\text{mg mL}^{-1}$ ) were dried under infrared lamp after coating on a  $\text{CaF}_2$  wafer that is subsequently placed in a variable path length cell with  $\text{CaF}_2$  windows.

### **Rheology**

The rheological properties of hydrogels were measured with a rotary rheometer (KINEXUS LAB+, Malvern Company, UK). The measurements were performed using a dynamic frequency sweep test with 0.1% strain over a range of frequencies (0.1-100 rad/s), a temperature controller was connected to the rheometer to maintain a temperature of 25  $^\circ\text{C}$ . Gels were freshly prepared by heating-cooling method or sonication methods and directly poured on the rheometer. Data acquisition was repeated

in triplicate, and average values were plotted.

### **Attenuated total reflectance Fourier transform infrared spectroscopy (ATR-FTIR)**

FTIR spectra were collected in transmission mode on a Thermofisher Nicolet iS5 FTIR spectrometer. Samples dissolved in DMSO-D<sub>6</sub> or organogels in ethanol-D<sub>6</sub> were placed on diamond ATR windows and covered with a Teflon spacer. For each sample 64 scans were collected from 1800 to 1500 cm<sup>-1</sup> and averaged in order to obtain a good signal-to-noise ratio. Spectra of DMSO-D<sub>6</sub> or ethanol-D<sub>6</sub> were collected as background and subtracted from the sample spectra.

### **Acknowledgments**

The authors thank the National Nature Science Foundation of China (NSFC 51833006), the Innovation Program of Shanghai Municipal Education Commission (201701070002E00061), the Science and Technology Commission of Shanghai Municipality (STCSM, No. 19441903000, 19ZR1425400), and SJTU Trans-med Awards Research (NO. WF540162603).

### **Declaration of Competing Interest**

The authors declare that they have no known competing financial interests or personal relationships that could have appeared to influence the work reported in this paper.

**Key words:** dipeptide, molecular chirality, self-assembly, chiral nanostructures, supramolecular organogel

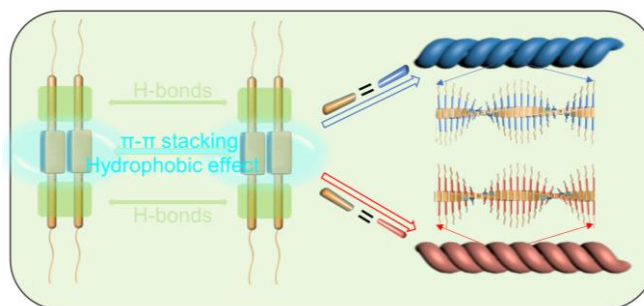
### **References**

- [1] M. Liu, L. Zhang and T. Wang, *Chem. Rev.* **2015**, *11*, 57304-7397.
- [2] H. Liu, B. Pang, R. Garces, R. Dervisoglu, L. Chen, L. Andreas and K. Zhang, *Angew. Chem. Int. Ed.* **2018**, *57*, 16323-16328.
- [3] P. Duan, H. Cao, L. Zhang and M. Liu, *Soft Matter* **2014**, *10*, 5428-5448.
- [4] A. Ajayaghosh, R. Varghese, S.J. George and C. Vijayakumar, *Angew. Chem. Int. Ed.* **2006**, *45*, 1141-1144.
- [5] S. Goskulwad, D.D. La, M.A. Kobaisi, S.V. Bhosale, V. Bansal, A. Vinu, K. Ariga and S.V. Bhosale, *Sci. Rep.* **2018**, *8*, 11220.
- [6] D.J. van Dijken, P. Stacko, M.C.A. Stuart, W.R. Browne and B.L. Feringa, *Chem. Sci.* **2017**, *8*, 1783-1789.
- [7] Z. Shen, Y. Sang, T. Wang, J. Jiang, Y. Meng, Y. Jiang, K. Okuro and T. Aida, *Nat. Commun.* **2019**,

- 10, 3976.
- [8] C. Hao, R. Gao, Y. Li, L. Xu, M. Sun, C. Xu and H. Kuang, *Angew. Chem. Int. Ed.* **2019**, 58, 7371-7374.
- [9] Y. Zhang, M. Qin, C. Zhao, X. Dou, C. Xing, M. Sun, X. Ma, C. Feng, *Carbon* **2020**, 165, 82-89.
- [10] M. Qin, Y. Zhang, J. Liu, C. Xing, C. Zhao, X. Dou, C. Feng, *Langmuir* **2020**, 36, 2524-2533.
- [11] J.Y. Liu, F. Yuan, X.Y. Ma, D.I.Y. Auphedeous, C.L. Zhao, C.T. Liu, C.Y. Shen, C.L. Feng, *Angew. Chem. Int. Ed.* **2018**, 57, 6475-6479.
- [12] H. Zheng, T. Yoshitomi, K. Yoshimoto, *ACS App. Bio-Mater.* **2018**, 1, 538-543.
- [13] A. Nitti, D. Pasini, *Adv. Mater.* **2020**, 1908021.
- [14] A.R. Palmans, E.W. Meijer, *Angew. Chem. Int. Ed.* **2007**, 46 8948-8968.
- [15] G. Liu, J. Sheng, H. Wu, C. Yang, G. Yang, Y. Li, R. Ganguly, L. Zhu, Y. Zhao, *J. Am. Chem. Soc.* **2018**, 140, 6467-6473.
- [16] M. Wang, P. Zhou, J. Wang, Y. Zhao, H. Ma, J.R. Lu, H. Xu, *J. Am. Chem. Soc.* **2017**, 139, 4185-4194.
- [17] E.E. Greciano, J. Calbo, J. Buendia, J. Cerda, J. Arago, E. Orti, L. Sanchez, *J. Am. Chem. Soc.* **2019**, 141, 7463-7472.
- [18] X. Zhang, J. Zou, K. Tamhane, F.F. Kobzeff, J. Fang, *Small* **2010**, 6, 217-20.
- [19] X. Lu, Z. Guo, C. Sun, H. Tian, W. Zhu, *J. Phy. Chem. B* **2011**, 115, 10871-10876.
- [20] A. Sánchez-Ferrer, J. Adamcik, R. Mezzenga, *Soft Matter* **2012**, 8, 149-155.
- [21] Y. Zhao, W. Yang, D. Wang, J. Wang, Z. Li, X. Hu, S. King, S. Rogers, J.R. Lu, H. Xu, *Small* **2018**, 14, 1703216.
- [22] C. Zhou, Y. Ren, J. Han, X. Gong, Z. Wei, J. Xie, R. Guo, *J. Am. Chem. Soc.* **2018**, 140, 9417-9425.
- [23] Y. Sang, P. Duan and M. Liu, *Chem. Commun.* **2018**, 54, 4025-4028.
- [24] S.T. Wang, Y. Lin, R.K. Spencer, M.R. Thomas, A.I. Nguyen, N. Amdursky, E.T. Pashuck, S.C. Skaalure, C.Y. Song, P.A. Parmar, R.M. Morgan, P. Ercius, S. Aloni and R.N. Zuckermann, *ACS nano* **2017**, 11, 8579-8589.
- [25] C. Li, K. Deng, Z. Tang, L. Jiang, *J. Am. Chem. Soc.* **2010**, 132, 8202-8209.
- [26] H. Choi, K.J. Cho, H. Seo, J. Ahn, J. Liu, S.S. Lee, H. Kim, C. Feng, J.H. Jung, *J. Am. Chem. Soc.* **2017**, 139, 17711-17714.
- [27] Z. Huang, S.K. Kang, M. Banno, T. Yamaguchi, D. Lee, C. Seok, E. Yashima and M. Lee, *Science* **2012**, 337, 1521-1526.
- [28] X. Zhu, Y. Li, P. Duan, M. Liu, *Chem. Eur. J.* **2010**, 16, 8034-8040.
- [29] M. Qin, Y. Li, Y. Zhang, C. Xing, C. Zhao, X. Dou, Z. Zhang, C. Feng, *Small* **2020**, e2004756.
- [30] H. Jiang, Y. Jiang, J. Han, L. Zhang and M. Liu, *Angew. Chem. Int. Ed.* **2019**, 58, 785-790.
- [31] Y. Wang, W. Qi, R. Huang, X. Yang, M. Wang, R. Su and Z. He, *J. Am. Chem. Soc.* **2015**, 137, 7869-7880.
- [32] A.J. Markvoort, H.M. ten Eikelder, P.A. Hilbers, T.F. de Greef and E.W. Meijer, *Nat. Commun.* **2011**, 2, 509.
- [33] H. Cao and S. De Feyter, *Nat. Commun.* **2018**, 9, 3416.
- [34] S.K. Jha, K.S. Cheon, M.M. Green and J.V. Selinger, *J. Am. Chem. Soc.* 1999, 121, 1665-1673.
- [35] T. Tachibana, H. Kambara, *J. Am. Chem. Soc.* **1965**, 87, 3015-3106.
- [36] Q. Xing, J. Zhang, Y. Xie, Y. Wang, W. Qi, H. Rao, R. Su and Z. He, *ACS Nano* **2018**, 12, 12305-12314.
- [37] X. Zhu, Y. Jiang, D. Yang, L. Zhang, Y. Li and M. Liu, *Chem. Sci.* **2019**, 10, 3873-3880.

- [38] Y. Li, A. Hammoud, L. Bouteiller and M. Raynal, *J. Am. Chem. Soc.* **2020**, *142*, 5676-5688.
- [39] S. Marchesan, C.D. Easton, K.E. Styan, L.J. Waddington, F. Kushkaki, L. Goodall, K.M. McLean, J.S. Forsythe, P.G. Hartley, *Nanoscale* **2014**, *6*, 5172-5180.
- [40] K. Basu, A. Baral, S. Basak, A. Dehsorkhi, J. Nanda, D. Bhunia, S. Ghosh, V. Castelletto, I.W. Hamley, A. Banerjee, *Chem. Commun.* **2016**, *52*, 5045-5048.
- [41] K.J. Nagy, M.C. Giano, A. Jin, D.J. Pochan and J.P. Schneider, *J. Am. Chem. Soc.* **2011**, *133*, 14975-14977.
- [42] S. Basak, I. Singh, A. Ferranco, J. Syed and H.B. Kraatz, *Angew. Chem. Int. Ed.* **2017**, *56*, 13288-13292.
- [43] J. Zhou, X. Du, J. Li, N. Yamagata, B. Xu, *J. Am. Chem. Soc.* **2015**, *137*, 10040-10043.
- [44] J. Shi, X. Du, D. Yuan, J. Zhou, N. Zhou, Y. Huang, B. Xu, *Biomacromolecules* **2014**, *15*, 3559-3568.
- [45] M.T. Jeena, K. Jeong, E.M. Go, Y. Cho, S. Lee, S. Jin, S.W. Hwang, J.H. Jang, C.S. Kang, W.Y. Bang, E. Lee, S.K. Kwak, S. Kim and J.H. Ryu, *ACS Nano* **2019**, *13*, 11022-11033.
- [46] L. Zhang, J. Qin, S. Lin, Y. Li, B. Li and Y. Yang, *Langmuir* **2017**, *33*, 10951-10957.
- [47] Y. Fu, B. Li, Z. Huang, Y. Li and Y. Yang, *Langmuir* **2013**, *29*, 6013-6017.
- [48] K. Lv, L. Zhang, W. Lu and M. Liu, *ACS Appl. Mater. Inter.* **2014**, *6*, 18878-18884.
- [49] X. Chen, Z. Huang, S.Y. Chen, K. Li, X.Q. Yu and L. Pu, *J. Am. Chem. Soc.* **2010**, *132*, 7297-7299.
- [50] N. Berova, L. Di Bari and G. Pescitelli, *Chem. Soc. Rev.* **2007**, *36*, 914-931.
- [51] H. Cao, X. Zhu and M. Liu, *Angew. Chem. Int. Ed.* **2013**, *52*, 4122-4126.
- [52] G.F. Liu, L.Y. Zhu, W. Ji, C.L. Feng and Z.X. Wei, *Angew. Chem. Int. Ed.* **2016**, *55*, 2411-2415.
- [53] G. Liu, X. Li, J. Sheng, P.Z. Li, W.K. Ong, S.Z.F. Phua, H. Agren, L. Zhu and Y. Zhao, *ACS Nano* **2017**, *11*, 11880-11889.
- [54] J. Sadlej, J.C. Dobrowolski, J.E. Rode, *Chem. Soc. Rev.* **2010**, *39*, 1478-1488.
- [55] K. McAulay, B. Dietrich, H. Su, M.T. Scott, S. Rogers, Y.K. Al-Hilaly, H. Cui, L.C. Serpell, A.M. Seddon, E.R. Draper, D.J. Adams, *Chem. Sci.* **2019**, *10*, 7801-7806.
- [56] R. Amemiya, M. Mizutani, M. Yamaguchi, *Angew. Chem. Int. Ed.* **2010**, *49*, 1995-1999.
- [57] X. Caumes, A. Baldi, G. Gontard, P. Brocorens, R. Lazzaroni, N. Vanthuyne, C. Troufflard, M. Raynal, L. Bouteiller, *Chem. Commun.* **2016**, *52*, 13369-13372.
- [58] V. Caplar, L. Frkanec, N. Sijakovic Vujicic, M. Zinic, *Chem. Euro. J.* **2010**, *16*, 3066-3082.
- [59] L. Wang, X. Jin, L. Ye, A.Y. Zhang, D. Bezuidenhout, Z.G. Feng, *Langmuir*, **2017**, *33*, 13821-13827.
- [60] K. Nagy-Smith, P.J. Beltramo, E. Moore, R. Tycko, E.M. Furst and J.P. Schneider, *ACS Cent. Sci.* **2017**, *3*, 586-597.
- [61] A. Ajayaghosh, C. Vijayakumar, R. Varghese and S.J. George, *Angew. Chem. Int. Ed.* **2006**, *45*, 456-460

## Table of Content



For C<sub>2</sub>-symmetrical dipeptide-based derivatives bearing various amino acid sequences and different chiralities, their supramolecular chirality is only determined by the amino acid adjacent to the benzene core and irrespective of the absolute configuration of C-terminal amino acid.